Meltwater Pulse 1A from Antarctica as a Trigger of the Bølling-Allerød Warm Interval

Andrew J. Weaver,[1]* Oleg A. Saenko,[1] Peter U. Clark,[2] Jerry X. Mitrovica[3]

Meltwater pulse 1A (mwp-1A) was a prominent feature of the last deglaciation, which led to a sea-level rise of ~20 meters in less than 500 years. Concurrent with mwp-1A was the onset of the Bølling-Allerød interstadial event (14,600 years before the present), which marked the termination of the last glacial period. Previous studies have been unable to reconcile a warm Northern Hemisphere with mwp-1A originating from the Laurentide or Fennoscandian ice sheets. With the use of a climate model of intermediate complexity, we demonstrate that with mwp-1A originating from the Antarctic Ice Sheet, consistent with recent sea-level fingerprinting inferences, the strength of North Atlantic Deep Water (NADW) formation increases, thereby warming the North Atlantic region and providing an explanation for the onset of the Bølling-Allerød warm interval. The established mode of active NADW formation is then able to respond to subsequent freshwater forcing from the Laurentide and Fennoscandian ice sheets, setting the stage for the Younger Dryas cold period.

The melting of continental ice sheets during the last deglaciation provided a freshwater source to the ocean that affected global sea level and the strength of the thermohaline circulation. An exceptionally large melting event, inferred from far-field relative sea-level records, occurred ~14,600 years before the present (yr B.P.) wherein global sea level rose by about 20 m in less than 500 years. The ice sheet that served as the source for this event, known as meltwater pulse 1A (mwp-1A), has been the subject of some controversy since mwp-1A was first identified from Barbados coral records (*1*). The Laurentide Ice Sheet is commonly cited as the most likely source for mwp-1A, but this raises the apparent conundrum of reconciling a large freshwater forcing {~0.5 sverdrup [1 sverdrup (Sv) = 10^6 m^3 s^{-1}] over several hundred years} to the North Atlantic Ocean with an active Atlantic thermohaline circulation and associated warm climate of the Bølling-Allerød warm interval (hereafter B-A) (*2*). Moreover, a satisfactory mechanism for the onset of the B-A event, conventionally considered as marking the termination of the last glacial period, has not been identified.

Clark *et al*. (*3*) provided compelling evidence that the partial collapse of the Antarctic Ice Sheet was responsible for a substantial component of mwp-1A. They noted that the ice-sheet ablation responsible for mwp-1A would lead to a sea-level fingerprint that is a dramatic departure from eustasy, due primarily to a reduction in the gravitational attraction of ocean water toward the location(s) of the source. A comparison of fingerprints predicted for various mwp-1A scenarios with available far-field relative sea-level records strongly supported an Antarctic source for mwp-1A and ruled out a sole Laurentide source for the event. Further evidence for an Antarctic source for mwp-1A comes from South Atlantic records of ice-rafted debris (IRD) derived from the Antarctic Ice Sheet, where Kanfoush *et al*. (*4*) document the existence of one such IRD event (SA0) that correlates to mwp-1A and the Antarctic Cold Reversal.

Here, we provide a comprehensive explanation for the cause of the B-A interstadial event in and around the North Atlantic as a consequence of mwp-1A. In particular, we show that an Antarctic source for mwp-1A of realistic magnitude and duration causes an increase in the intensity of the North Atlantic thermohaline circulation, which in turn increases temperatures in the North Atlantic region. On removal of the freshwater forcing, the strength of the North Atlantic overturning converges to present-day levels over the course of 1000 years.

Mwp-1A age. A U/Th age of 14,235 ± 100 yr B.P. on a Barbados sample of *Acropora palmata* has been conventionally used to constrain the start of mwp-1A (*5*). On this basis, mwp-1A is inferred to have occurred after, and possibly in response to, the onset of the B-A at 14,600 yr B.P. (*6*). However, several lines of evidence indicate that mwp-1A was synchronous with the B-A. These results would appear to be inconsistent with the constraint that *A. palmata* only lives in waters less than 6 m deep and thus that the 14,235-yr-B.P. sample requires sea level to have risen only 5.5 m since 14,690 ± 85 yr B.P., which is the age of the next older Barbados sample. This is only the case, however, when the rate of sea-level rise is <15 mm $year^{-1}$. If sea-level rise is >15 mm $year^{-1}$, *A. palmata* will be unable to grow vertically at the same rate and the coral will either try to catch up or give up, depending on the rate of sea-level rise (*7*). In either case, if mwp-1A began at 14,600 yr B.P., the 14,235-yr-B.P. coral no longer constrains water depths to be <6 m and instead it may have lived at a much greater depth (*8*).

A radiocarbon-dated relative sea-level record from the Sunda Shelf indicates that mwp-1A began ~300 ^{14}C years earlier than suggested by the Barbados record of radiocarbon-dated coral (*9*) (Fig. 1A). Some of this difference may result from the Barbados corals living at water depths >6 m because they were unable to grow at the rate of sea-level rise during mwp-1A. Many of the Sunda Shelf data, on the other hand, are based on in situ mangrove root remains, which constrain sea level to within 2 m (*9*) and thus represent a more robust indicator of sea level, particularly during times of rapid sea-level change.

An additional explanation for the discrepancy between the Barbados and Sunda Shelf radiocarbon-dated sea-level records may be that the 400-year reservoir age applied to the Barbados samples is too large (*9*). We evaluate this further by noting that a Barbados coral sample with paired ^{14}C (reservoir-corrected) and U/Th dates (12,200 ± 100 ^{14}C yr B.P.; 14,235 ± 100 U/Th yr B.P.) is younger than the Cariaco calibration curve by 200 ^{14}C years (*10*). The Cariaco record agrees well with the terrestrial Lake Suigetsu record (*11*), suggesting that the reservoir correction at Cariaco is correct and that the reservoir correction for Barbados corals at this time is thus too large by ~200 years. A reduced reservoir correction of 200 years for the six Barbados samples that date between 12,600 and 12,700 ^{14}C yr B.P. results in excellent agreement between the Barbados and Sunda Shelf data and suggests that mwp-1A began between 12,400 and 12,500 ^{14}C yr B.P. (Fig. 1B).

An age of 12,400 to 12,500 ^{14}C yr B.P. for the start of mwp-1A places the event in a 900-year-long radiocarbon plateau that corresponds to the start of the B-A. Specifically, a large increase in the Atlantic thermohaline circulation

[1]School of Earth and Ocean Sciences, University of Victoria, Post Office Box 3055, Victoria, British Columbia V8W 3P6, Canada. [2]Department of Geosciences, Oregon State University, Corvallis, OR 97331, USA. [3]Department of Physics, University of Toronto, Toronto, Ontario M5S 1A7, Canada.

*To whom correspondence should be addressed. E-mail: weaver@uvic.ca

that was responsible for the 150 per mil decrease in atmospheric radiocarbon (and thus the plateau) (*12*) also caused the B-A warming. Additional evidence in support of synchroneity is provided from the South China Sea, where proxy records demonstrate rapid flooding of the sea at the same time as abrupt warming of sea-surface temperatures during the B-A (*13*).

Climate model and results. Our experiments were conducted with version 2.4 of the UVic Earth System Climate Model (*14*, *15*). The coupled model has been extensively and successfully evaluated against contemporary climate observations (*14*, *16*) as well as paleoclimate proxy records (*17*, *18*). Similar to other models (*19*, *20*), the UVic model reveals at least two stable modes of the global thermohaline circulation under present-day conditions. These modes correspond to the states with and without North Atlantic Deep Water (NADW) formation (Fig. 2, A and B), referred to as "on" and "off" modes, respectively. The "on" mode is representative of the present-day climate and is characterized by a much warmer North Atlantic than the "off" mode (Fig. 2C) because of the northward transport of heat by the active thermohaline circulation. The "off" mode is representative of NADW formation in response to a Heinrich event (*21*) and was responsible for the Oldest Dryas cold interval that immediately preceded the onset of the B-A (*22*).

In Experiment (Exp.) 1, a transition from the stable present-day 'on' mode to the 'off' mode is triggered by imposing a freshwater perturbation to the North Atlantic (region A; Fig. 2C). This experiment was designed to obtain an initial climate state without NADW formation such as the state that characterized the North Atlantic region after Heinrich event 1 (H1) and before the onset of the B-A. The fresh water was gradually discharged at a rate linearly increasing from 0 to 0.2 Sv over 1000 years (i.e., 100 Sv years), which was enough to cause the cessation of NADW formation. A subsequent reduction of the freshwater perturbation in this experiment at the same rate (i.e., from 0.2 Sv back to 0 Sv over 1000 years), although slightly increasing the surface density in the source region of NADW, did not lead to a restart of NADW formation, indicating the well-known existence of a hysteresis behavior (*18*, *20*, *23*). Moreover, fixing the external freshwater flux at 0 Sv and integrating the model forward for several thousand years also did not result in a restart of NADW formation, indicating that the "off" mode is stable.

One common feature of the two modes of the Atlantic thermohaline circulation is a recirculation of Antarctic Bottom Water (AABW) within the Atlantic (Fig. 2, A and B). However, the circulation of NADW and Antarctic Intermediate Water (AAIW) is quite different (Fig. 2, A and B). In the present-day climate, a relationship between the potential densities (ρ) of these water masses is

$$\rho_{AABW} > \rho_{NADW} > \rho_{AAIW} \quad (1)$$

Accordingly, AAIW and the upper thermocline waters feed the formation of NADW, which sinks in the North Atlantic. However, a discharge of a large enough amount of fresh water within the Atlantic can change the above potential density relationship to (Fig. 3A) $\rho_{AABW} > \rho_{AAIW} > \rho_{NADW}$. As a result, AAIW is denser than NADW, which intensifies the inflow of fresh AAIW into the Atlantic and the compensating outflow of saline thermocline water from the Atlantic, leading to an additional freshening of the Atlantic. Thus, the formation of NADW fully collapses to the "off" mode, whereas a circulation cell at intermediate depths originating from the Southern Ocean is established (Fig. 2B).

In order to switch from the "off" back to the "on" mode, a change in the potential density relationship between AAIW and NADW must be triggered, i.e., to $\rho_{NADW} > \rho_{AAIW}$. This can be achieved either by applying a negative freshwater perturbation to a region within the Atlantic (*23*–*27*) or by applying a positive freshwater perturbation in

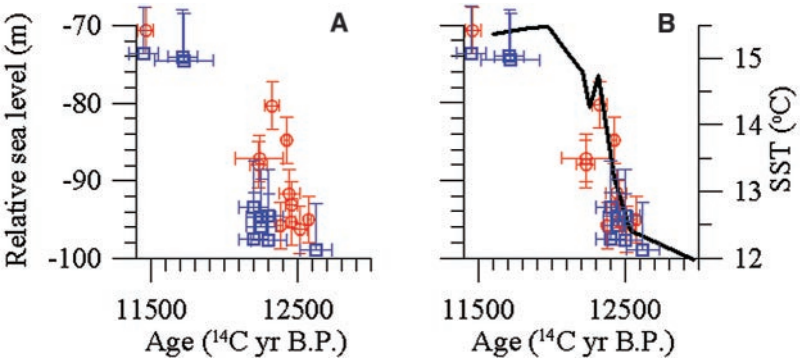

Fig. 1. (**A**) Relative sea-level data dated by radiocarbon from Barbados (blue squares) (*5*, *38*) and Sunda Shelf (red circles) (*9*). The Barbados coral data have a 400-year reservoir age correction. Seven of the Sunda data points represent weighted mean ages and errors of two radiocarbon ages that were obtained from the same core either at the same depth or within 15 cm of each other. The original radiocarbon ages thus weighted were either within 1 SD of each other or stratigraphically inverted. (**B**) The same relative sea-level data from Barbados and Sunda Shelf, but the six radiocarbon-dated corals from Barbados with original uncorrected ages between 12,600 and 12,700 ^{14}C yr B.P. are now plotted with a 200-year reservoir age. The black line represents sea-surface temperatures derived from alkenones from core SU81-18 off the coast of Portugal (*39*). This record suggests that the onset of the B-A was characterized by a 3°C increase in sea-surface temperatures over ~500 years, which is similar to our modeled response (Fig. 4E).

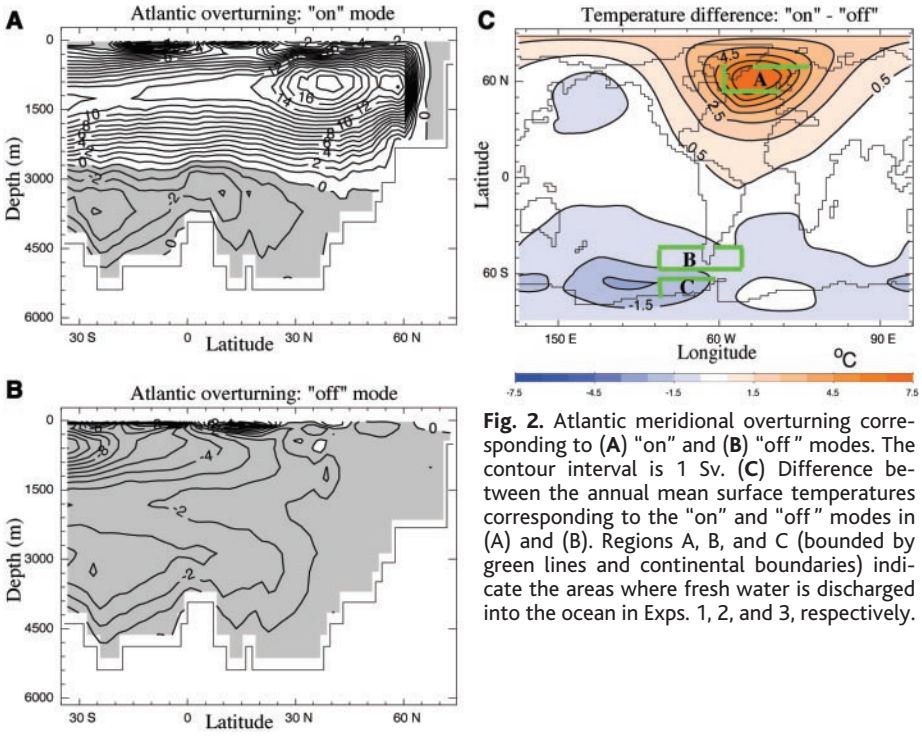

Fig. 2. Atlantic meridional overturning corresponding to (**A**) "on" and (**B**) "off" modes. The contour interval is 1 Sv. (**C**) Difference between the annual mean surface temperatures corresponding to the "on" and "off" modes in (A) and (B). Regions A, B, and C (bounded by green lines and continental boundaries) indicate the areas where fresh water is discharged into the ocean in Exps. 1, 2, and 3, respectively.

the Southern Ocean (*28*, *29*) that would effectively make the AAIW fresher. The latter approach is illustrated below in two sensitivity experiments as a simulation of mwp-1A originating in the Southern Hemisphere.

In Exp. 2, we started from the "off" state and discharged fresh water to the region around the southern tip of South America (region B; Fig. 2C). The freshwater perturbation has a linear shape, increasing from 0 to 1 Sv over 500 years, implying a net freshwater perturbation of 250 Sv years. The associated global sea-level rise by year 500 is 22 m. After year 500, the freshwater perturbation is set to zero and the model is integrated for a further 1000 years. Experiment 3 was identical to Exp. 2, except the freshwater perturbation was applied to the region west of the Antarctic Peninsula (region C; Fig. 2C). We note that the region around the southern tip of South America is an area of enhanced AAIW and Subantarctic Mode Water formation (*30*, *31*). The region to the west of Antarctic Peninsula is also important for AAIW formation, at least in our model (*32*), and is also downstream of the West Antarctic Ice Sheet, which is a possible candidate for the freshwater source associated with mwp-1A.

As a result of the freshwater discharge into regions B and C, a transition from the "off" to the "on" state is triggered. The density in the source region of AAIW formation begins to decline (Fig. 3B). Furthermore, the density in the source region of NADW increases, even though no perturbation other than to regions B and C is applied in the corresponding experiments. Rather, the increase of the density in the source region of NADW is because of the gradual intensification of NADW formation (Fig. 4E). This constitutes a positive feedback between the overturning circulation and the salinity in the North Atlantic first described by Stommel (*33*). Specifically, the intensified formation of NADW advects more saline subtropical waters to the northern North Atlantic, which increases surface density there and further intensifies the overturning circulation. An important difference between the two experiments is the reduction of density in the Ross Sea in Exp. 3, which contributes to the overall reduction of surface density over the regions of AABW formation (i.e., Ross and Weddell Seas) (Fig. 3B).

By year 500, the formation of NADW reaches, respectively, 10 Sv and 12.5 Sv in Exps. 2 and 3 (Fig. 4, A, B, and E), warming up the North Atlantic by as much as 4°C and 5°C, respectively, in good agreement with the SU81-18 sea-surface temperature record off Portugal (Fig. 1B). At the same time, large areas of the Southern Hemisphere cool by as much as 7°C (Fig. 4, C to E), consistent with the seesaw response of the NADW overturning (*12*). In

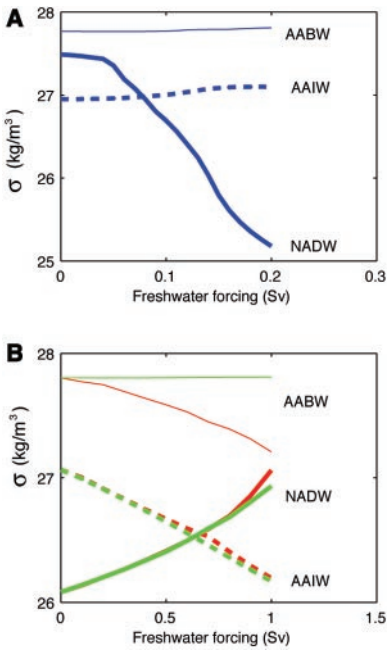

Fig. 3. Surface density ($\sigma = \rho - 1000$) in the source regions of NADW formation (North Atlantic), AAIW formation (southeast Pacific and southwest Atlantic), and AABW formation (Weddell and Ross Seas) as a function of freshwater perturbation in (**A**) Exp. 1 and (**B**) Exps. 2 (green) and 3 (red).

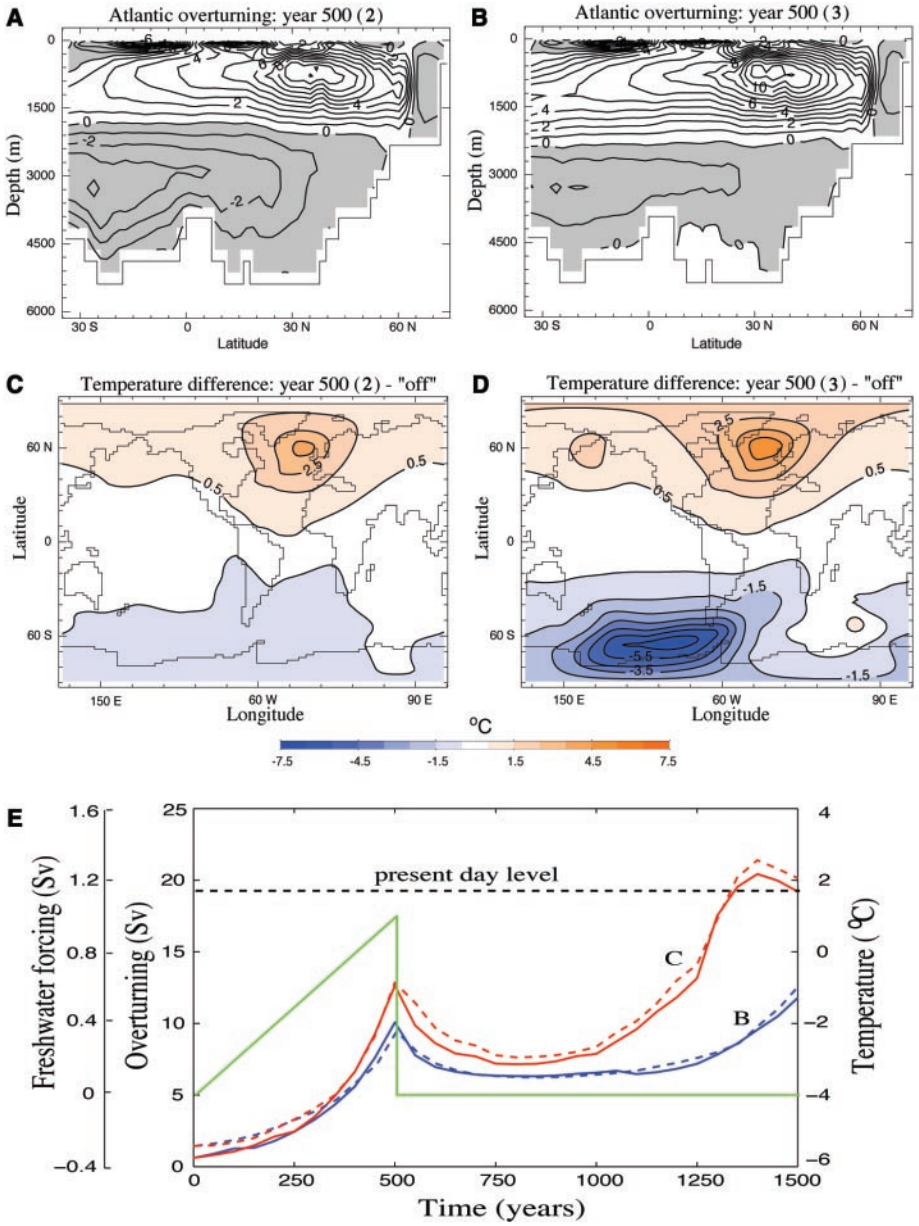

Fig. 4. Atlantic meridional overturning at year 500 in (**A**) Exp. 2 and (**B**) Exp. 3. Surface air temperature difference between year 500 [(A) and (B)] and the "off" mode (Fig. 2B) for (**C**) Exp. 2 and (**D**) Exp. 3. (**E**) Time series of the freshwater perturbation (green), maximum Atlantic overturning (solid), and North Atlantic surface air temperature were averaged over the ocean between 45°W and 9°E, 58.5°N and 65.7°N (dashed). Blue, Exp. 2; red, Exp. 3. The dashed black line gives the present-day overturning strength and surface air temperature in the "on" mode (Fig. 2A).

agreement with the above-noted reduction of AABW density in Exp. 3, the circulation cell associated with AABW weakens. This contributes to the different quantitative responses of the North Atlantic climate in Exps. 2 and 3 to the freshwater perturbations originating in the Southern Ocean.

On termination of the freshwater discharge in the Southern Ocean, the formation of NADW first reduces and hence so does the near-surface air temperature in the North Atlantic (Fig. 4E). However, the production of NADW does not collapse. Rather, about 500 years after the freshwater forcing is terminated, the rate of NADW formation begins to intensify (Fig. 4E). By year 1500, it exceeds the pretermination rate of NADW formation (at year 500) in Exp. 2 and reaches the present-day ("on" mode) level in Exp. 3 (Fig. 4E).

Summary and conclusions. The results of these experiments suggest a strong interhemispheric link between the global thermohaline circulation and the formation of global-scale water masses. We conclude that, by applying freshwater perturbations (of magnitude similar to mwp-1A) to the regions of AAIW formation, it is possible to trigger a transition from the "off" to the "on" mode of NADW formation. This, in turn, causes increased heat transport into the North Atlantic and subsequent warming there as well as cooling in the Southern Hemisphere, providing a compelling mechanism for onset of the B-A warm interval in the north and the Antarctic Cold Reversal in the south.

The mechanism behind the reestablishment of active NADW formation is straightforward. In the present-day climate, Eq. 1 shows that NADW has a potential density between that of AABW and AAIW. As a consequence, AAIW and upper thermocline waters feed the formation of NADW. Either the discharge of fresh water into the Atlantic or the extraction of fresh water from the AAIW formation regions in the south can cause AAIW to be denser than NADW. This then intensifies the inflow of fresh AAIW into the Atlantic and the compensating outflow of saline thermocline water from the Atlantic, which leads to a positive feedback to North Atlantic freshening. The result is a complete collapse of NADW formation. To restart NADW formation, the density of NADW surface waters must be increased to be greater than that of AAIW surface waters. This can be accomplished either by freshening the AAIW formation region or by extracting fresh water from the NADW formation region. We consider the former as an explanation for the onset of the B-A.

By reconciling the climatic relation between mwp-1A and the onset of the B-A, our results provide a comprehensive explanation for the sea level and climatic events during the last deglaciation (Fig. 5). Before mwp-1A, NADW formation was in an "off" state as a consequence of H1 (*22*). During the corresponding Oldest Dryas cold period (Fig. 5A), the rate of global sea-level rise was on the order of 2.3 mm year^{-1} (Fig. 5B), indicating little melting of ice sheets. Subsequently, during mwp-1A, sea level rose at rates exceeding 40 mm year^{-1} (Fig. 5B). We suggest that mwp-1A occurred in response to a prolonged interval of Southern Hemisphere warming that began ~19,000 yr B.P. (Fig. 5C) (*34*). Some of this warming may have originated from the large reduction in Atlantic thermohaline circulation triggered by H1 ~17,500 yr B.P. and the corresponding bipolar seesaw (*12*, *22*), with the concurrent global rise in CO_2 (*35*) and methane (*34*) amplifying the warming before mwp-1A. In any event, this warming may have triggered a partial collapse of the Antarctic Ice Sheet, perhaps by destabilizing ice shelves.

By freshening the AAIW formation region, mwp-1A then caused warming in the north (the B-A) and cooling in the south (the Antarctic Cold Reversal) (Fig. 5C). The rate of sea-level rise during the B-A warm period was ~17 mm year^{-1} (Fig. 5B), less than that during mwp-1A but substantially higher than that during the Oldest Dryas cold period. Most of this sea-level rise likely originated from melting of Northern Hemisphere ice sheets in response to the B-A warming. This increased freshwater flux to the North Atlantic may have preconditioned the Atlantic thermohaline circulation so that subsequent routing of fresh water through the St. Lawrence River (*36*, *37*) caused a large reduction in the Atlantic thermohaline circulation and the attendant Younger Dryas cold period. During the Younger Dryas, the rate of sea-level rise decreased to ~3 mm year^{-1} (Fig. 5B), representing a large decrease in melting of ice sheets and corresponding freshwater flux to the North Atlantic. As a result, when fresh water routed through the St. Lawrence River was subsequently diverted to other outlets (*36*, *37*), the Atlantic thermohaline circulation strengthened again, marking the end of the Younger Dryas. Sea level then rose at ~11 mm year^{-1} (Fig. 5B) for the remainder of the deglaciation.

Finally, we note that other events or mechanisms that change the salinity of the AAIW formation region may have similarly affected NADW formation at other times. For example, Kanfoush *et al.* (*4*) identified several IRD events derived from Antarctica between 30 and 55 kyr B.P. that are associated with high benthic $\delta^{13}C$ values, indicating increased NADW formation and inferred North Atlantic warming. Within dating uncertainties, their IRD events SA3, SA4, and SA5 occurred subsequent to Southern Hemisphere warming events A1, A2, and A3, respectively (*34*). Accordingly, if these IRD events record substantial ice loss from Antarctica, they may represent a similar response of the Antarctic Ice Sheet to regional warming, with attendant effects on the thermohaline circulation and North Atlantic climate such as those we document for mwp-1A during the last deglaciation.

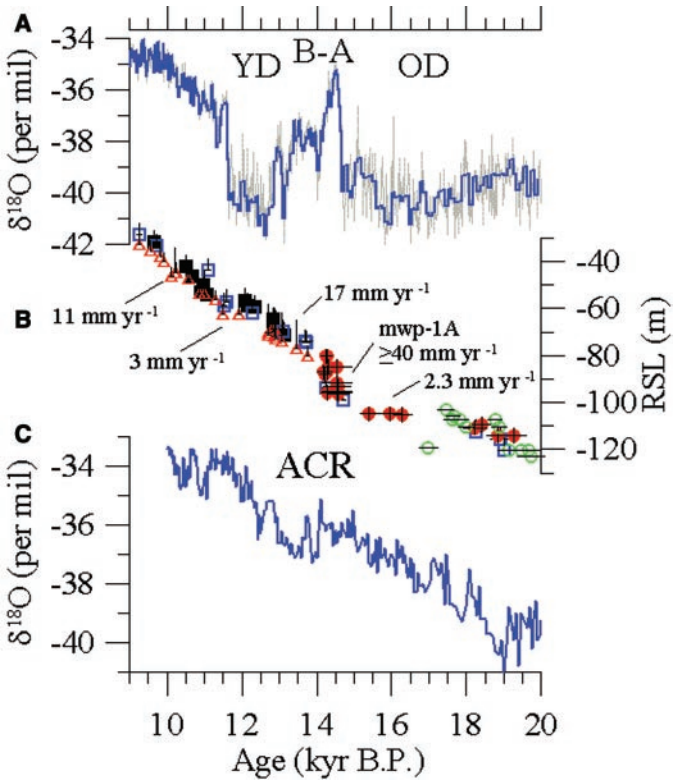

Fig. 5. Climate and sea-level records spanning the last deglaciation. (**A**) The Greenland Ice Sheet Project 2 (GISP2) oxygen isotope record (*40*, *41*). OD is the Oldest Dryas cold period, and YD is the Younger Dryas cold period. (**B**) Relative sea-level (RSL) records from far-field sites. Also shown are average rates of sea-level rise for the periods 19 to 14.6, 14.6 to 14.1, 14.1 to 12.9, 12.9 to 11.6, and 11.6 to 6 kyr B.P. Data are from Bonaparte Gulf (green open circles) (*42*), Barbados U/Th dated corals (open blue squares) (*5*), Sunda Shelf (*9*), Tahiti (open red triangles) (*5*), and New Guinea (closed black squares) (*43*). (**C**) The Byrd ice-core oxygen isotope record on the GISP2 time scale (*34*). ACR is the Antarctic Cold Reversal.

References and Notes

1. R. G. Fairbanks, *Nature* **342**, 637 (1989).
2. P. U. Clark *et al.*, *Paleoceanogr.* **11**, 563 (1996).
3. P. U. Clark, J. X. Mitrovica, G. A. Milne, M. E. Tamisiea, *Science* **295**, 2438 (2002).
4. S. L. Kanfoush *et al.*, *Science* **288**, 1815 (2000).

5. E. Bard, B. Hamelin, R. G. Fairbanks, A. Zindler, *Nature* **345**, 405 (1990).
6. E. Bard *et al.*, *Nature*, **382**, 241 (1996).
7. L. F. Montaggioni *et al*., *Geology* **25**, 555 (1997).
8. Two U/Th ages on *A. palmata* were obtained from near the top of Barbados core RGF-9: 14,690 ± 85 yr B.P. (RGF9-13-3) and 14,230 ± 100 yr B.P. (RGF9-8-2). When the long-term uplift rate of Barbados is accounted for (0.34 m/kyear) (*1*), the difference in elevation between the two samples represents a relative sea-level rise of 5.5 m. However, given the conventional water-depth uncertainty constrained by this species (within 6 m of sea level), a maximum rise in relative sea level of 11.5 m, or more than half the rise associated with mwp-1A, is possible. The youngest dated sample of *A. palamata* (RGF9-8-2) is overlain by deep-water species *Porites astroides* and *A. cervicornis*, suggesting that the 14,230 kyr B.P. horizon was already in the process of drowning in response to rapidly rising sea level. This sample may thus have been well below its normal 6-m water-depth tolerance at the time it grew, allowing more than 11.5 m of relative sea-level rise since 14,690 ± 85 yr B.P.
9. T. Hanebuth, K. Stattegger, P. M. Grootes, *Science* **288**, 1033 (2000).
10. K. A. Hughen, J. R. Southon, S. J. Lehman, J. T. Overpeck, *Science* **290**, 1951 (2000).
11. H. Kitigawa, J. van der Plicht, *Radiocarbon* **42**, 369 (2000).
12. P. U. Clark, N. G. Pisias, T. F. Stocker, A. J. Weaver, *Nature* **415**, 863 (2002).
13. M. Kienast, T. J. J. Hanebuth, C. Pelejero, S. Steinke, *Geology* **31**, 67 (2003).
14. A. J. Weaver *et al*., *Atmosphere-Ocean* **39**, 361 (2001).
15. The model consists of a three-dimensional (3D) ocean general circulation model (GCM) coupled to a thermodynamic-dynamic sea ice model and an energy-moisture balance atmosphere model. A reduced-complexity atmosphere model is used for computational efficiency. Atmospheric heat transport is parameterized through Fickian diffusion, and moisture transport is accomplished through both advection and diffusion, with precipitation occurring when the relative humidity exceeds 85%. The atmospheric dynamical feedback option has not been included in this application. Precipitation over land instantaneously returns to the ocean via 1 of 33 river basins unless it falls as snow, in which case it is locally retained until it melts. The atmospheric model includes a parameterization of water vapor–planetary longwave feedbacks, although the radiative forcing associated with changes in atmospheric CO_2 is externally imposed as a reduction of the planetary long-wave radiative flux. The ocean component of the coupled model is a fully nonlinear 3D ocean GCM with a global resolution of 3.6° (zonal) by 1.8° (meridional) and 19 vertical levels. It includes the parameterization of Gent and McWilliams to represent the effect of mixing associated with mesoscale eddies. The sea-ice model incorporates an elastic-viscous-plastic rheology representation of dynamics, a two-category thickness distribution, and ice-snow thermodynamics. The model resolves the annual cycle, and the incoming solar radiation at the top of the atmosphere depends on the orbital parameters. One of the virtues of the coupled model is that we do not need to use explicit flux adjustments to keep the simulation of the present climate stable.
16. O. A. Saenko, A. Schmittner, A. J. Weaver, *J. Phys. Oceanogr.* **32**, 3376 (2002).
17. A. Schmittner, K. J. Meissner, M. Eby, A. J. Weaver, *Paleoceanogr.* **17** (**2**), 1015, doi:10.1029/2001PA-000633 (2002).
18. A. Schmittner, M. Yoshimori, A. J. Weaver, *Science* **295**, 1489 (2002).
19. S. Manabe, R. J. Stouffer, *Tellus* **51A**, 400 (1999).
20. S. Rahmstorf, *Clim. Dyn.* **12**, 799 (1996).
21. A. J. Weaver, *Geophys. Monogr. Am. Geophys. Union* **112** (American Geophysical Union, Washington, DC, 1999), pp. 285–300.
22. R. B. Alley, P. U. Clark, *Ann. Rev. Earth Planet. Sci.* **27**, 149 (1999).
23. T. F. Stocker, D. G. Wright, *Nature* **351**, 729 (1991).
24. A. F. Fanning, A. J. Weaver, *Paleoceanogr.* **12**, 307 (1997).
25. E. Maier-Reimer, U. Mikolajewicz, in *Oceanography*, A. Ayala-Castanares, W. Wooster, A. Yanez-Arancibia, Eds. (Universidad Nacional Autónoma de México Press, Mexico City, Mexico, 1989), pp. 87–99.
26. A. Schiller, U. Mikolajewicz, R. Voss, *Clim. Dyn.* **13**, 325 (1997).
27. S. Manabe, R. J. Stouffer, *Paleoceanogr.* **12**, 321 (1997).
28. U. Mikolajewizc, *Ann. Glaciol.* **27**, 311 (1998)
29. D. Seidov, B. J. Haupt, E. J. Barron, M. Maslin, *Geophys. Monogr. Am. Geophys. Union* **126** (American Geophysical Union, Washington, DC, 2001), pp. 147–168.
30. M. H. England, J. S. Godfrey, A. C. Hirst, M. Tomczak, *J. Phys. Oceanogr.* **23**, 1553 (1993).
31. M. S. McCartney, *Deep-Sea Res.* **24**, 103 (1977).
32. O. A. Saenko, A. J. Weaver, M. H. England, *J. Phys. Oceanogr.*, in press.
33. H. M. Stommel, *Tellus* **13**, 224 (1961).
34. T. Blunier, E. J. Brook, *Science* **291**, 109 (2001).
35. E. Monnin *et al*., *Science* **291**, 112 (2001).
36. W. S. Broecker *et al*., *Nature* **341**, 318 (1989).
37. P. U. Clark *et al*., *Science* **293**, 283 (2001).
38. E. Bard, M. Arnold, R. G. Fairbanks, B. Hamelin, *Radiocarbon* **35**, 191 (1993).
39. E. Bard, F. Rostek, J.-L. Turon, S. Gendreau, *Science* **289**, 1321 (2000).
40. P. M. Grootes, M. Stuiver, J. W. C. White, S. J. Johsen, J. Jouzel, *Nature* **366**, 552 (1993).
41. M. Stuiver, P. M. Grootes, *Quat. Res.* **53**, 277 (2000).
42. Y. Yokoyama, K. Lambeck, P. De Deckker, P. Johnston, K. Fifield, *Nature* **406**, 713 (2000).
43. R. L. Edwards, H. Cheng, M. T. Murrell, S. J. Goldstein, *Science* **260**, 962 (1993).

44. We are grateful for funding from the Natural Sciences and Engineering Research Council via the operating and Climate System History and Dynamics programs and for research support from the Canadian Foundation for Climate and Atmospheric Sciences. This research was also made possible through support from the Killam Foundation and the Canada Research Chair program to A.J.W. and from the Earth System History Program of NSF to P.U.C. We also acknowledge discussions with J. Gregory and M. Kienast and are grateful for the insightful comments of two anonymous reviewers.

2 December 2002; accepted 28 January 2003

Spread of HTLV-I Between Lymphocytes by Virus-Induced Polarization of the Cytoskeleton

Tadahiko Igakura,[1,3] Jane C. Stinchcombe,[4] Peter K. C. Goon,[1] Graham P. Taylor,[2] Jonathan N. Weber,[2] Gillian M. Griffiths,[4] Yuetsu Tanaka,[5] Mitsuhiro Osame,[3] Charles R. M. Bangham[1]*

Cell contact is required for efficient transmission of human T cell leukemia virus–type 1 (HTLV-I) between cells and between individuals, because naturally infected lymphocytes produce virtually no cell-free infectious HTLV-I particles. However, the mechanism of cell-to-cell spread of HTLV-I is not understood. We show here that cell contact rapidly induces polarization of the cytoskeleton of the infected cell to the cell-cell junction. HTLV-I core (Gag protein) complexes and the HTLV-I genome accumulate at the cell-cell junction and are then transferred to the uninfected cell. Other lymphotropic viruses, such as HIV-1, may similarly subvert normal T cell physiology to allow efficient propagation between cells.

The human T cell leukemia virus–type 1 (HTLV-I) is an oncogenic exogenous retrovirus that infects between 10 and 20 million people worldwide. Of these infected individuals, 2 to 3% develop adult T cell leukemia/lymphoma (*1*), and a further 2 to 3% develop a variety of chronic inflammatory syndromes, most notably HTLV-I–associated myelopathy/tropical spastic paraparesis (HAM/TSP) (*2*, *3*).

HTLV-I is transmitted between individuals by transfer of infected lymphocytes in breast milk, semen, or blood (*4*). Transfusion with cell-free blood products appears to carry a negligible risk of HTLV-I infection (*5*) . In vitro, efficient spread of HTLV-I infection also requires cell contact (*6*, *7*). Cell contact is required because lymphocytes naturally infected with HTLV-I produce very few cell-free HTLV-I virions and because, of the virions that are released, only 1 in 10^5 to 10^6 is infectious (*8*, *9*).

The mechanism of cell-to-cell spread of HTLV-I is not understood. HTLV-I expresses a surface glycoprotein, the envelope (Env) protein, which is required for infectivity (*9*) and for cell-cell fusion and syncytium formation (*10*–*12*). Env is presumed to bind to a cellular receptor for HTLV-I, but the receptor has not yet been identified (*13*, *14*). Certain integrins, including intercellular and vascular cell-adhesion molecules ICAM-1, ICAM-3, and VCAM, act as cofactors for HTLV-I–induced cell fusion (*15*, *16*).

In this study we tested the hypothesis that HTLV-I is transmitted directly across the cell-cell junction. We used confocal microscopy to examine the distribution of HTLV-I Gag and Env proteins and the HTLV-I genome in fresh, unstimulated peripheral blood mononuclear cells (PBMCs) isolated directly from

[1]Department of Immunology, [2]Department of Genito-Urinary Medicine and Communicable Diseases, Imperial College London, St. Mary's Campus, Norfolk Place, London W2 1PG, UK. [3]The Third Department of Internal Medicine, Faculty of Medicine, Kagoshima University, 8-35-1 Sakuragaoka, Kagoshima 890-8520, Japan. [4]Sir William Dunn School of Pathology, University of Oxford, Oxford OX1 3RE, UK. [5]Department of Infectious Disease and Immunology, Okinawa-Asia Research Center of Medical Science, Faculty of Medicine, University of the Ryukyus, Uehara-cho 207, Nishihara, Okinawa 903-0215, Japan.

*To whom correspondence should be addressed. E-mail: c.bangham@imperial.ac.uk